J Mater Sci: Mater Med (2015) 26:72
DOI 10.1007/s10856-015-5408-4

BIOCOMPATIBILITY STUDIES

Osseointegration improvement by plasma electrolytic oxidation of modified titanium alloys surfaces

Mónica Echeverry-Rendón · Oscar Galvis · David Quintero Giraldo · Juan Pavón · José Luis López-Lacomba · Emilio Jiménez-Piqué · Marc Anglada · Sara M. Robledo · Juan G. Castaño · Félix Echeverría

Received: 9 April 2014 / Accepted: 6 November 2014 / Published online: 29 January 2015

Abstract Titanium (Ti) is a material frequently used in orthopedic applications, due to its good mechanical properties and high corrosion resistance. However, formation of a non-adherent fibrous tissue between material and bone drastically could affect the osseointegration process and, therefore, the mechanical stability of the implant. Modifications of topography and configuration of the tissue/material interface is one of the mechanisms to improve that process by manipulating parameters such as morphology and roughness. There are different techniques that can be used to modify the titanium surface; plasma electrolytic oxidation (PEO) is one of those alternatives, which consists of obtaining porous anodic coatings by controlling parameters such as voltage, current, anodizing solution and time of the reaction. From all of the above factors, and based on previous studies that demonstrated that bone cells sense substrates features to grow new tissue, in this work commercially pure Ti (c.p Ti) and Ti6Al4V alloy samples were modified at their surface by PEO in different anodizing solutions composed of H_2SO_4 and H_3PO_4 mixtures. Treated surfaces were characterized and used as platforms to grow osteoblasts; subsequently, cell behavior parameters like adhesion, proliferation and differentiation were also studied. Although the results showed no significant differences in proliferation, differentiation and cell biological activity, overall results showed an important influence of topography of the modified surfaces compared with polished untreated surfaces. Finally, this study offers an alternative protocol to modify surfaces of Ti and their alloys in a controlled and reproducible way in which biocompatibility of the material is not compromised and osseointegration would be improved.

M. Echeverry-Rendón (✉) · S. M. Robledo
Programa de Estudio y Control de Enfermedades Tropicales (PECET), Instituto de Investigaciones Médicas, Facultad de Medicina, Universidad de Antioquia, Calle 70 No. 52-21, Medellín, Colombia
e-mail: monica.echeverry@udea.edu.co; monicaecheverryr@gmail.com

M. Echeverry-Rendón · O. Galvis · D. Quintero Giraldo · J. G. Castaño · F. Echeverría
Centro de Investigación, Innovación y Desarrollo de Materiales (CIDEMAT), Facultad de Ingeniería, Universidad de Antioquia, Calle 70 No. 52-21, Medellín, Colombia

J. Pavón
Grupo de Biomateriales Avanzados y Medicina Regenerativa (BAMR), Programa de Bioingeniería, Facultad de Ingeniería, Universidad de Antioquia, Calle 70 No. 52-21, Medellín, Colombia

J. L. López-Lacomba
Grupo de Ingeniería de Tejidos, Estudios Biofuncionales, Universidad Complutense, Paseo Juan XXIII, 28040 Madrid, Spain

E. Jiménez-Piqué · M. Anglada
Centro de Integridad Estructural y Fiabilidad de los Materiales, CIEFMA, Universidad Politécnica de Cataluña, Avda. Diagonal 647 (ETSEIB), 08028 Barcelona, Spain

1 Introduction

Osseous tissue is exposed to damages due to degenerative or traumatic diseases that can cause severe disability and, therefore, high economic and social costs [1–3]. However, the life quality of patients could be improved by using biomaterials that may interact with biological systems having minimal flaws and long service; therefore, they may be used for manufacturing human body implants [4]. Alloplastic implants using synthetic biomaterials have become a good choice because of their high immunological

compatibility, easy way to obtain, and high availability in the materials commercial market [5]. Nevertheless, materials used in vivo must have similar characteristics and properties with respect to bone hosting tissue, and should also promote osseointegration; this means, to reach a direct, structural and functional connection between bone and implant surface [6].

Titanium (Ti) alloys are the materials currently used to replace and improve the functionality of human bones due to their high biocompatibility, low elastic modulus, reasonable high mechanical strength, and good corrosion resistance in biological environments [7, 8]. The physicochemical properties of Ti surfaces are given by an oxide layer composed mainly of TiO_2, which is naturally formed on the metal when this is in contact with air at room temperature [9]. This TiO_2 layer is responsible for the good behavior of Ti alloys when used as biomaterials and placed in contact with physiological environments [10]. However, despite their notable advantages, the bioinert nature of these materials could be involved in the production of non-adherent fibrous tissue at the bone-material biointerface, affecting in some cases the implant stability and increasing the risk of the implant loosening over time [11]. Several studies have shown that surface properties such as porosity, roughness, hydrophobic/hydrophilic characteristics, texture, morphology, composition and free surface energy are important factors to stimulate cells adhesion, morphological changes, and enhancing cells proliferation and differentiation around the implant as well [12–14].

Various surface modification techniques such as sol–gel [15, 16], chemical vapor deposition (CVD) [17], hydrothermal [18], and anodic oxidation [19–21] have been used to obtain layers of TiO_2 and to improve the surface properties of Ti alloys. Among the anodic oxidation methods to produce anodic TiO_2 layers, electrolytic plasma oxidation (PEO) also called micro arc oxidation, is an economic, effective and useful technique widely used and studied in the last decade. This method allows anodic growth of layers that exhibit greater thickness, variation in crystallinity, morphology, and composition, which are characteristics that depend on both electrical parameters of anodizing and electrolyte composition. In addition, the adhesion to the substrate, even using surfaces with complex geometries, is improved [7, 22–24]. Porous anodic layers may be obtained by PEO using H_2SO_4, H_3PO_4 and H_2O_2 as electrolytes, which help apatite to deposit on their surfaces when they are immersed in simulated body fluid solution (SBF) [25, 26]. This behavior is caused by the incorporation of phosphorus into the oxide layers from electrolyte [27–29]. After this process, in vivo and in vitro assays have allowed some researchers to report improvements in implants of Ti, biocompatibility associated to surfaces that were previously treated by different techniques; in these studies, micro-roughness and incorporation of species within the anodic layers were responsible of higher biocompatibility [10, 12, 30, 31].

In this study, samples of c.p Ti and Ti6Al4V alloy were treated by PEO using sulphuric acid solutions containing different concentrations of phosphoric acid. The anodic layers obtained were evaluated to determine if the modification could affect the behavior of the bone cells by biological studies. Osteoblastic cell lines Saos-2 and UMR-106 were grown in the obtained surfaces. These cells were chosen because they have similar features to osteoblastic cells regarding to differentiation process. In addition, the relationships between cell interaction and surface morphologies, composition, and roughness of the oxide of titanium coating were also studied. Cell morphology, adhesion, proliferation and mineralization of cells that were in contact with the modified surfaces, were used as criteria to identify the processing conditions that could improve the biological performance of the osteoblastic cells in the processes associated with osseointegration.

2 Materials and methods

2.1 Material processing

2.1.1 Plasma electrolytic oxidation (PEO) coatings

Cylindrical samples (1.2 mm of thickness) of commercially pure titanium (c.p Ti grade 2, purity 99.6 %, ASTM F-67-13 [32]) and Ti6Al4V alloy (ELI, ASTM F-136-12 [33]), were cut from a rod of 20 mm of diameter. All specimens were mechanically polished with silicon carbide paper (120, 240, 320, 400 and 600 grades), and then degreased with acetone in an ultrasonic bath for 15 min. Subsequently, the samples were soaked in a solution mixture of HF (3 %) and HNO_3 (30 %) for 15 s according to ASTM B-600-11 standard [34], in order to remove the natural formed oxide layer, and finally they were washed with distilled water and dried with cold air.

All specimens were processed in phosphoric/sulphuric acid mixtures as anodizing solutions, at room temperature and without stirring. Mixtures of 0.1 M H_3PO_4/1.5 M H_2SO_4, 0.3 M H_3PO_4/1.5 M H_2SO_4, 0.6 M H_3PO_4/1.5 M H_2SO_4 and 0.9 M H_3PO_4/1.5 M H_2SO_4 were used for c.p Ti samples; whereas for Ti6Al4V alloy the solutions used were 0.3 M H_3PO_4/1.5 M H_2SO_4, 0.6 M H_3PO_4/1.5 M H_2SO_4, 0.9 M H_3PO_4/1.5 M H_2SO_4 and 0.6 M H_3PO_4/0.9 M H_2SO_4. To obtain the anodic coatings on both materials, PEO process was conducted in two sequential steps: First a current density of 35 mA/cm^2 was applied, and when the potential reached 180 V the process was continued in potentiostatic mode at this voltage value for

all specimens; however, for the sample obtained in 0.1 M H_3PO_4/1.5 M H_2SO_4, the mode change was performed at 160 V. Three of these electrolytes and anodizing conditions were similar to those reported by Lee et al. [26]. The process was developed in a two-electrode electrochemical cell, a titanium cylinder with an area of 7 cm^2 was set as anode and a platinum mesh was used as cathode. A DC power supply (Kepco BHK 500-0.4 MG) was used to obtain the anodic coatings. The voltage data were recorded electronically by Labview 8.1 software (National Instruments) interfaced with a personal computer. After anodization, the specimens were removed immediately from the electrolyte; subsequently, they were rinsed with deionized water in ultrasound bath for 15 min to clean the surface, and finally dried in cold air.

2.1.2 Characterization of PEO coatings

The surface morphologies of the anodic coatings were observed by scanning electron microscopy (SEM) using a JEOL JSM 6940 LV equipped with an energy dispersive X-ray (EDS) analyzer. The phases present in the samples were determined by X-ray diffraction (XRD), using a Philips XPERT-MPD (PW3050) XRD instrument with Cu Kα radiation ($\alpha = 0.15405$ nm) at 45 kV and 40 mA. The incident angle was fixed at 3°, the scanning speed was 0.00625° s^{-1}, with a step size of 0.05° and a scan range from 15° to 85° (in 2θ). The Raman spectra were acquired on a micro-Raman Horiba-Jobin-Yvon spectrometer system. Specimens were illuminated through a 50× objective using the 632.81 nm excitation from a He–Ne laser source with a pinhole of 800 μm and a slit of 200 μm. Focused ion beam (FIB) analysis was carried out to characterize the cross sectional microstructure, as well as the chemical composition of the anodic layers, through a Carl-Zeiss Neon40 equipment by using decreasing ion currents until 50 pA at 30 kV. Observations were done in a field emission scanning electron microscope (FE-SEM). Confocal laser was used to analyze the surface roughness of the anodic layers using a LEXT-OLS Serie Standard type equipment (resonant galvano-mirror scanner mode and high speed, high precision auto focus unit).

2.2 Biological assays

2.2.1 Osteoblast cell lines

Human osteoblastic cell line Saos-2 (HTB-85, ATCC), rat osteoblastic cell line UMR-106 (CRL-1661, ATTC) and mouse myoblast cell line C2C12 (CRL-1772, ATCC) were used in the different assays as described below. Saos-2 cells were grown in a McCoy medium (Sigma) while UMR-106 and C2C12 cells were grown in DMEM medium (Gibco). All mediums were supplemented with 10 % fetal bovine serum (FBS, Gibco), 1 % penicillin/streptomycin and cells were incubated at 37 °C in humidified atmosphere containing 5 % CO_2.

2.2.2 Cytotoxicity assay

The potential toxicity of the c.p Ti and Ti6Al4V alloy with and without surface modification were evaluated by using the 3-(4,5-dimethylthiazol-2-yl)-2,5-diphenyltetrazolium-bromide (MTT) assay, in which insoluble formazan is produced as indicator of cell viability. The following specimens were tested: c.p Ti samples treated with 0.1 M H_3PO_4/1.5 M H_2SO_4, 0.3 M H_3PO_4/1.5 M H_2SO_4, 0.6 M H_3PO_4/1.5 M H_2SO_4 and 0.9 M H_3PO_4/1.5 M H_2SO_4 and Ti6Al4V treated with 0.3 M H_3PO_4/1.5 M H_2SO_4, 0.6 M H_3PO_4/1.5 M H_2SO_4, 0.9 M H_3PO_4/1.5 M H_2SO_4 and 0.6 M H_3PO_4/0.9 M H_2SO_4. For both materials polished samples without any modification were also evaluated. In this assay, Saos-2 cells were seeded on the top of each specimen at a concentration of 10,000 cells/cm^2 and incubated at 37 °C, with 5 % CO_2, during 72 h. Next, 10 μl of MTT solution was added and the cells were incubated at 37 °C for 4 h. After that, crystals of formazan were dissolved by addition of sodium dodecyl (SDS) and optical density (O.D) was measured at 570 nm by using of a spectrophotometer (Benchmark, Biorad); cells incubated in absence of samples were considered as control. Results were performed in triplicate and normalized according to the value obtained for the control which was considered as 0 % of cytotoxicity.

2.2.3 Proliferation assay

Cell proliferation was determined by Alamar Blue assay (Invitrogen). For this purpose, UMR-106 osteoblast line cell were seeded at a concentration of 10,000 cells/cm^2 on the top of samples anodized with 0.1 M H_3PO_4/1.5 M H_2SO_4 solution for c.p Ti samples and 0.3 M H_3PO_4/1.5 M H_2SO_4 and 0.6 M H_3PO_4/0.9 M H_2SO_4 for the samples of the Ti6Al4V alloy. Cells were incubated at 37 °C, with 5 % CO_2 for 4 days and quantification of the cell grow was performed each 24 h. For that, the quantity of viable cells was measured by addition of Alamar Blue solution at a 1:10 ratio. Culture plates were incubated at 37 °C by 90 min and then fluorescence was read in a spectrophotometer (Biotek FL-600) with an excitation wavelength of 530 nm and an emission wavelength of 590 nm. Fluorescence values were corrected in relation to the average blank. Samples without any treatment (polished) were also evaluated. Results were normalized according to the value obtained for control cells. Assays were performed in triplicate.

2.2.4 Cellular morphology

Saos-2 cells at a density of 10,000 cells/cm^2 were grown on c.p Ti anodized samples with 0.1 M H_3PO_4/1.5 M H_2SO_4, 0.3 M H_3PO_4/1.5 M H_2SO_4, 0.6 M H_3PO_4/1.5 M H_2SO_4 and 0.9 M H_3PO_4/1.5 M H_2SO_4 and Ti6Al4V alloys samples anodized with 0.3 M H_3PO_4/1.5 M H_2SO_4, 0.6 M H_3PO_4/1.5 M H_2SO_4, 0.9 M H_3PO_4/1.5 M H_2SO_4, 0.6 M H_3PO_4/0.9 M H_2SO_4. After 72 h of incubation, cells were fixed with 2 % glutaraldehyde overnight at 4 °C and then specimens were washed three times with phosphate buffered saline (PBS), after that cells were dehydrated in increasing ethanol concentrations (30, 50, 70, 80, 90 and 100 %) followed by critical-point-dried (Samdri-795). Finally, samples were sputter-coated with gold (Dentom-Vacuum Desk IV), and observed under SEM. Images were obtained at an acceleration voltage of 15 kV at 50×, 250×, 500×, 1000×, 2000× and 5000× of magnification. Additionally, cells grown on the sample anodized with 0.1 M H_3PO_4/1.5 M H_2SO_4 were visualized by FIB. For this purpose, a cross section was created on a dual beam system Strata DB235 (FEI Company). Cells and surface were observed using a FE-SEM at a working distance of 5.3 mm, 1000× magnification, 15 kV acceleration voltage and 30 kV to 5 pA of energy current.

2.2.5 Cellular adhesion

UMR-106 osteoblasts at a concentration of 10,000 cell/cm^2 were grown on c.p Ti anodized with 0.1 M H_3PO_4/1.5 M H_2SO_4 and Ti6Al4V alloys treated with 0.3 M H_3PO_4/1.5 M H_2SO_4 and 0.6 M H_3PO_4/0.9 M H_2SO_4. After 4 h of incubation at 37 °C with 5 % of CO_2, Alamar Blue assay (Invitrogen) was performed. In this case, the supernatant from each well was transferred to other plate to recover non-adherent cells. Fresh medium was added to each well followed of addition of Alamar Blue solution in a 1:10 ratio. Plates were incubated at 37 °C, 5 % CO_2 for 90 min. After that, the fluorescence was read in a spectrofluorometer (Biotek FL-600) by using an excitation wavelength of 530 nm and emission wavelength of 590 nm. The values obtained were compared with cells grown on plastic where adhesion was considered optimal. Assays were performed in triplicate.

2.2.6 Configuration of the cytoskeleton

Saos-2 cells were seeded in culture conditions and during 72 h at a concentration of 10,000 cells/cm^2 on c.p Ti anodized treated with 0.1 M H_3PO_4/1.5 M H_2SO_4, 0.3 M H_3PO_4/1.5 M H_2SO_4, 0.6 M H_3PO_4/1.5 M H_2SO_4 or 0.9 M H_3PO_4/1.5 M H_2SO_4 and on Ti6Al4V alloys anodized treated with 0.3 M H_3PO_4/1.5 M H_2SO_4, 0.6 M H_3PO_4/1.5 M H_2SO_4, 0.9 M H_3PO_4/1.5 M H_2SO_4, 0.6 M H_3PO_4/0.9 M H_2SO_4. After that, cells were fixed with 3.8 % of paraformaldehyde during 20 min at 37 °C and treated with 5 mM ammonium chloride. Next, cells were treated with 0.25 % of Triton X-100. Nonspecific binding sites were blocked with 5 % FBS in PBS during 30 min at 37 °C. Finally, cytoskeleton and nucleus were labeled by using of Phalloidin-TRITC (P1951, Sigma) and 4′,6-diamodino-2-phenylindole dihydrochloride—DAPI (D9542, Sigma). Cells were observed under fluorescence microscope (Nikon LABOPHOT-2) at 10X and 40X magnification.

2.2.7 Mineralization

UMR-106 osteoblasts (10,000 cell/cm^2) were seeded over c.p Ti and Ti6Al4V alloy samples in presence of mineralized medium composed by DMEM (Invitrogen), 10 % BFS (Invitrogen), 1 mM de β sodium Glycerophosphate (Sigma), 50 μg/ml of ascorbic acid (Sigma) and 10^{-8} M of Dexamethasone (Sigma). After 4 and 7 days cells were fixed with ethanol and stained with alizarin red to detect mineralization zones. C2C12 cells were used as negative control. Staining with alizarin red allowed the visualization of calcium deposits from the osteoblasts on the samples of titanium by using of alight microscopy Olympus BX-100.

2.3 Statistical analysis

ANOVA and Bonferroni's post analysis were used to determine statistical significant differences according to anodizing conditions and control specimens at 0.05 level of significance by using GraphPad PrismVersion 6 software.

3 Results

3.1 Characterization of titanium oxide films

The increase in voltage and gas evolution in the first seconds of the process is observed, as well as color changes of the substrate surface as the system voltage increased. These variations are due to the formation of an oxide layer with thicknesses ranging from ten to a few hundred nanometers. The variation in color depends on the thickness, due to interference phenomena that occurs among the oxide, substrate and visible light [35, 36]. Numerous sparks of small size were detected after voltage had reached approximately 120 V, associated with localized breakdowns of the anodic layer. The sparks gradually covered the whole coating surface, causing color change from a faint pink to grey at the final stages; in addition, the density of sparks decreased whereas their size increased. These

observations are in agreement with results reported in the literature for PEO process [23, 37].

The surface morphology of anodic coatings obtained on c.p Ti and Ti6Al4V alloy specimens are shown in Fig. 1. Uniformly distributed circular and connected pores were formed on the surface of c.p Ti specimens anodized with 0.1 M H_3PO_4/1.5 M H_2SO_4 and 0.3 M H_3PO_4/1.5 M H_2SO_4 (Fig. 1 a, b). When H_3PO_4 concentration was increased in the electrolytes, a mixture of circular and elongated pores was observed on c.p Ti (Fig. 1c, d) and the pore sizes gradually increased. In this context, Oh et al. [25] and Lee et al. [26] reported the dependence of the layer's surface morphology on the electrolyte composition. By using an image analyzer, they found that the pore diameter of cell structures increases both with anodic time and concentration of phosphoric acid in the electrolyte. For the case of Ti6Al4V specimens, elongated pores and grooved morphology were obtained for all conditions analyzed in the present study (Fig. 1d–h).

Roughness analysis indicates an influence of the electrolyte concentration used on R_a values for all anodic coatings. As shown in Table 1, the surface of all coatings became rougher in comparison to the original roughness before the PEO process for both materials. In general, only small variations in roughness were obtained with the increase of H_3PO_4 content in the electrolytes. The coating

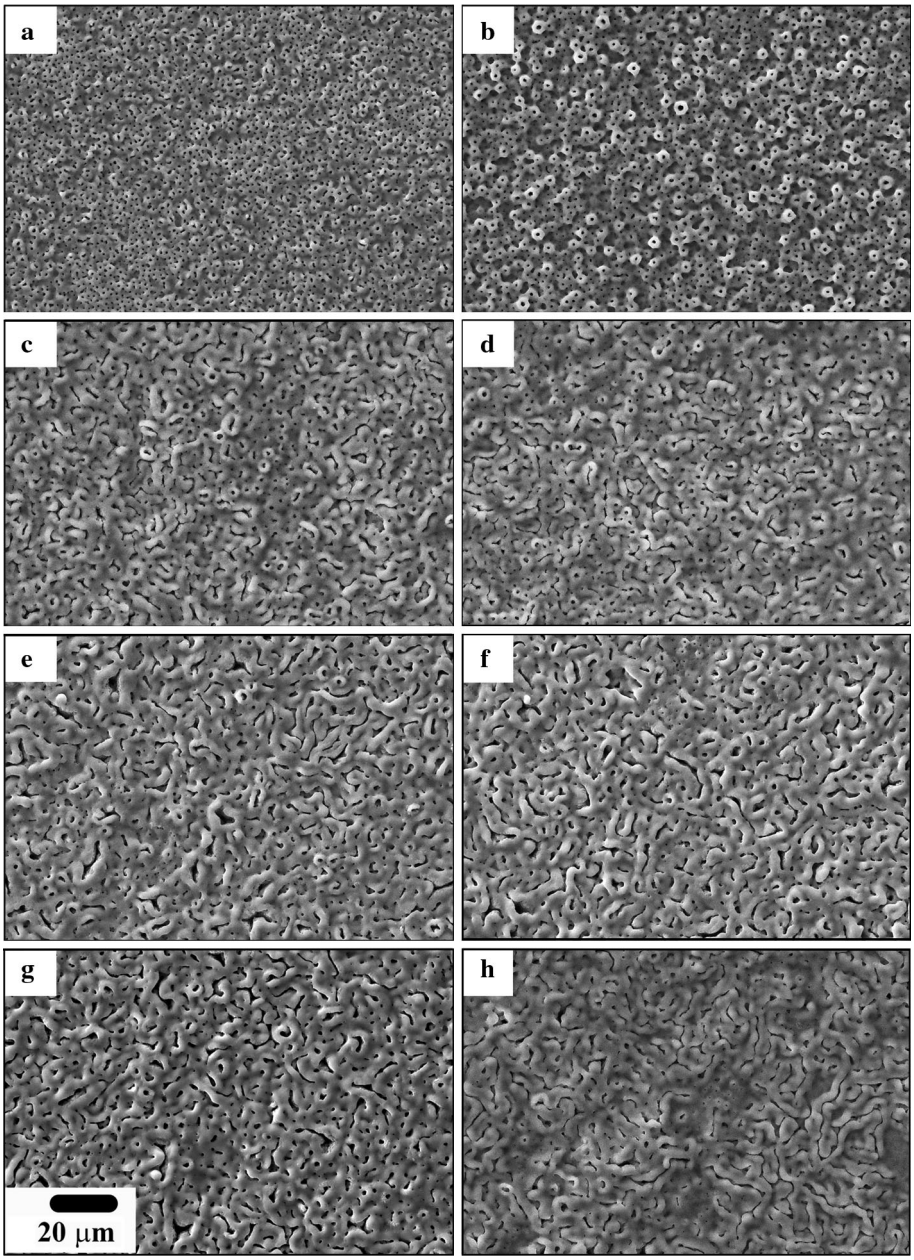

Fig. 1 SEM micrographs of anodic coatings formed on c.p Ti in **a** 0.1 M H_3PO_4/1.5 M H_2SO_4, **b** 0.3 M H_3PO_4/1.5 M H_2SO_4, **c** 0.6 M H_3PO_4/1.5 M H_2SO_4, **d** 0.9 M H_3PO_4/1.5 M H_2SO_4 and on Ti6Al4V in **e** 0.3 M H_3PO_4/1.5 M H_2SO_4, **f** 0.6 M H_3PO_4/1.5 M H_2SO_4, **g** 0.9 M H_3PO_4/1.5 M H_2SO_4, **h** 0.6 M H_3PO_4/0.9 M H_2SO_4, at 35 mA cm^{-2}

Table 1 Roughness (Ra) of the anodized surfaces and both substrates

Electrolyte	Roughness c.pTi Ra (μm)	Roughness Ti6Al4V Ra (μm)
Substrate before PEO process	0.198 ± 0.002	0.126 ± 0.001
0.1 M H_3PO_4/1.5 M H_2SO_4	0.270 ± 0.01	ND
0.3 M H_3PO_4/1.5 M H_2SO_4	0.427 ± 0.001	0,410 ± 0.004
0.6 M H_3PO_4/1.5 M H_2SO_4	0.383 ± 0.001	0,455 ± 0.003
0.9 M H_3PO_4/1.5 M H_2SO_4	0,392 ± 0.0003	0,395 ± 0.003
0.6 H_3PO_4/0.9 M H_2SO_4	ND	0,477 ± 0.0001

ND no data

obtained in 0.1 M H_3PO_4/1.5 H_2SO_4 on c.p Ti showed the lowest roughness among the anodic coatings ($R_a = 0.27 \pm 0.01$ μm), while the coating obtained on Ti6Al4V alloy in 0.6 M H_3PO_4/0.9 H_2SO_4 was the highest value of R_a (0.4772 ± 0.0001 μm).

Cross-section views of anodic coatings obtained on c.p Ti and Ti6Al4V alloy are shown in Fig. 2; images showed in Fig. 2a–e were obtained by FIB, whereas the remaining images (Fig. 2f–h) were mechanically prepared. These images clearly show the porous structure inside the coatings, which are mostly interconnected, typical of PEO coatings [37, 38]; in addition, for all coatings, porosity decreases as concentration of phosphoric acid (H_3PO_4) in the electrolyte increases. Roughness increase of the substrate/coating interface due to H_3PO_4 concentration variation was also observed. In Fig. 2c, d–g, h), it is observed that pores formation is related with an increased roughness at the substrate/coating interface, as black arrows indicate.

EDS analysis indicated that the amount of phosphorus incorporated into the coatings also increases with the concentration of H_3PO_4 in the electrolyte. On the other side, the thickness of coatings shows a slight trend to decrease with the increase of phosphoric acid concentration in the electrolyte. Results of elemental composition by EDS and average thickness values for each specimen on both substrates are shown in Table 2.

Diffraction patterns of anodic coatings formed on c.p Ti and Ti6Al4V are shown in Fig. 3a, b, respectively; these results indicate that anodic coatings consist exclusively of anatase [39]. In addition, it is observed that peaks intensity for anatase gradually decrease with the increase of phosphoric acid concentration; this could be associated to reduction of the average thickness of PEO coating as the phosphoric acid concentration increased. It has been also reported that the ionic species incorporated into the coatings from the solution are involved in the reactions leading to the formation of the anatase phase and these species are also correlated with the crystallization of the coatings [25, 26].

Micro-Raman spectra of PEO coatings obtained on c.p Ti and Ti6Al4V alloy samples treated in different electrolytes are shown in Fig. 4a, b. All spectra show the characteristic bands of titanium dioxide (TiO_2), specifically anatase phase 144, 397, 516 and 641 cm^{-1} [40–42]; there is no evidence of other phases, which confirms the XRD results. Similar to those results, the higher the phosphoric acid concentration, the lower the signals intensity, which again indicates thinner coatings forms at electrolytes containing more phosphoric acid.

3.2 Biological characterization

3.2.1 Effect of anodizing process on toxicity and cellular viability

Indicators of possible toxicity were obtained from measurements of mitochondrial activity of osteoblasts seeded on the different anodized samples. Cells seeded on plastic cell-culture were considered as control. Results were normalized according to the value obtained for the control. There was no significant difference between the control and anodized samples (Fig. 5).

3.2.2 Effect of anodizing process on cell adhesion, morphology and cytoskeletal organization

Cell-material interaction was evaluated after observation of pictures obtained with SEM, in which spatial distribution of osteoblast on the samples was studied. After 72 h of culture, a monolayer was formed covering most of the surface of the samples. Cells with a cuboidal shape and elongated extensions of cytoplasm (filopodia) were observed. This morphology is characteristic of osteoblasts and it allows an intimal interaction between substrate materials and cells by incrementing the contact area. Cell confluence was observed in c.p Ti and Ti6Al4V alloys polished to mirror finishing samples; however, cells with filopodia were scarce. A trend of cells growing in the same orientation of the polishing tracks was observed in both coated and untreated specimens (Fig. 6).

Cell–cell and cell–material interactions were evidenced by cytoplasmic prolongations that varied according to roughness of material. Cells showed a preference for binding to the edges of pores. More filopodia were observed in samples with smaller porous size, which for c.p Ti correspond to samples treated with 0.1 M H_3PO_4/1.5 M

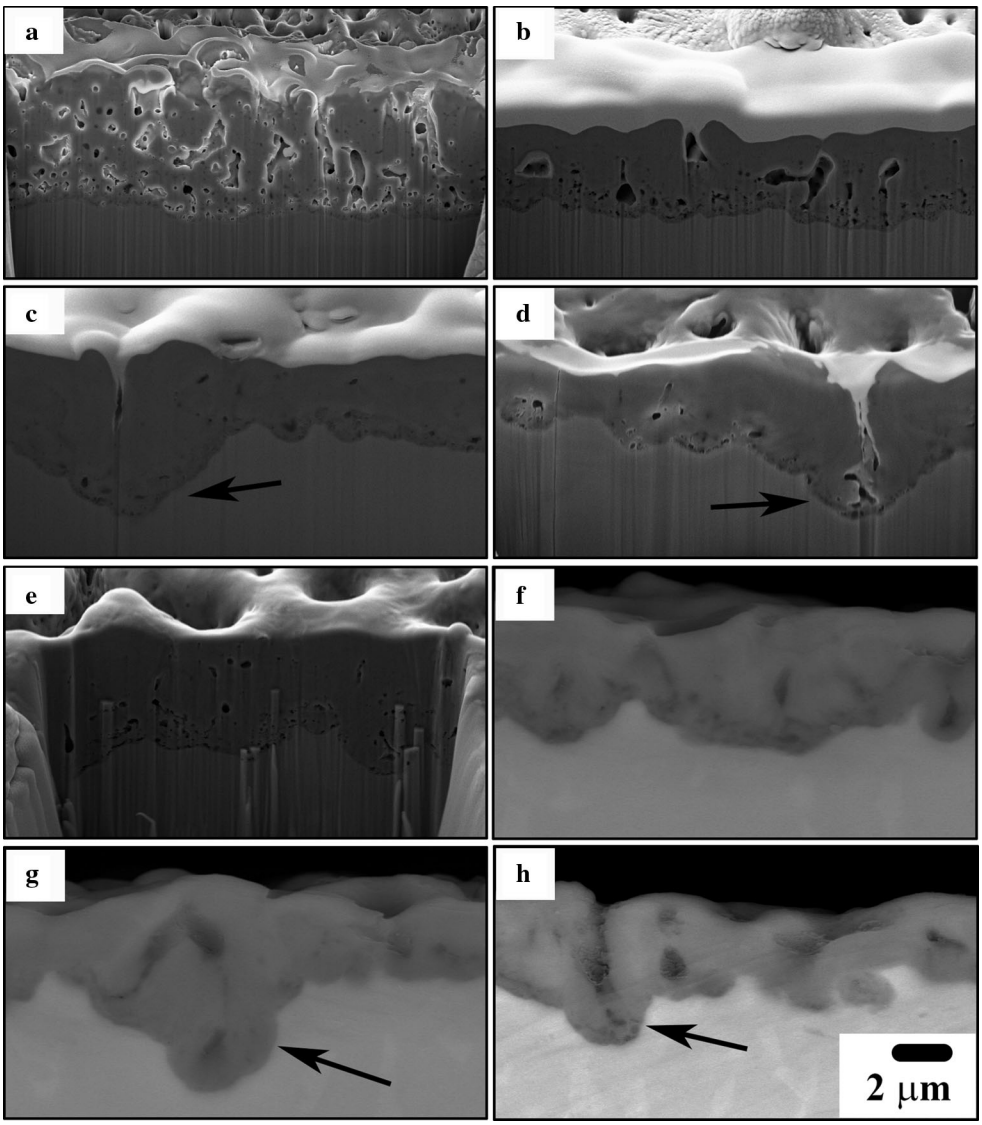

Fig. 2 FIB/SEM micrographs of cross-sections of anodic coatings formed on c.p Ti in **a** 0.1 M H_3PO_4/1.5 M H_2SO_4, **b** 0.3 M H_3PO_4/1.5 M H_2SO_4, **c** 0.6 M H_3PO_4/1.5 M H_2SO_4, **d** 0.9 M H_3PO_4/1.5 M H_2SO_4 and on Ti6Al4V in **e** 0.3 M H_3PO_4/1.5 M H_2SO_4, **f** 0.6 M H_3PO_4/1.5 M H_2SO_4, **g** 0.9 M H_3PO_4/1.5 M H_2SO_4, **h** 0.6 M H_3PO_4/0.9 M H_2SO_4, at 35 mA cm^{-2}

Table 2 Elemental composition and average thickness of anodic coatings obtained on c.p Ti and Ti6Al4V alloy

	Electrolyte	Atomic % Ti	Atomic % O	Atomic % P	Atomic % Al	Average thickness (μm)
c.p Ti	0.1 M H_3PO_4/1.5 M H_2SO_4	27.72	67.98	3.94	–	2.06 ± 0.11
	0.3 M H_3PO_4/1.5 M H_2SO_4	29.58	63.99	6.43	–	1.52 ± 0.12
	0.6 M H_3PO_4/1.5 M H_2SO_4	24.35	66.67	7.56	–	1.41 ± 0.53
	0.9 M H_3PO_4/1.5 M H_2SO_4	20.68	71.16	8.98	–	1.44 ± 0.57
Ti6Al4V	0.3 M H_3PO_4/1.5 M H_2SO_4	17.19	69.03	6.91	1.77	1.82 ± 0.18
	0.6 M H_3PO_4/1.5 M H_2SO_4	17.50	72.39	8.24	1.88	1.80 ± 0.34
	0.9 M H_3PO_4/1.5 M H_2SO_4	18.70	65.98	9.19	1.46	1.63 ± 0.77
	0.6 M H_3PO_4/0.9 M H_2SO_4	19.86	70.09	7.97	1.67	1.58 ± 0.33

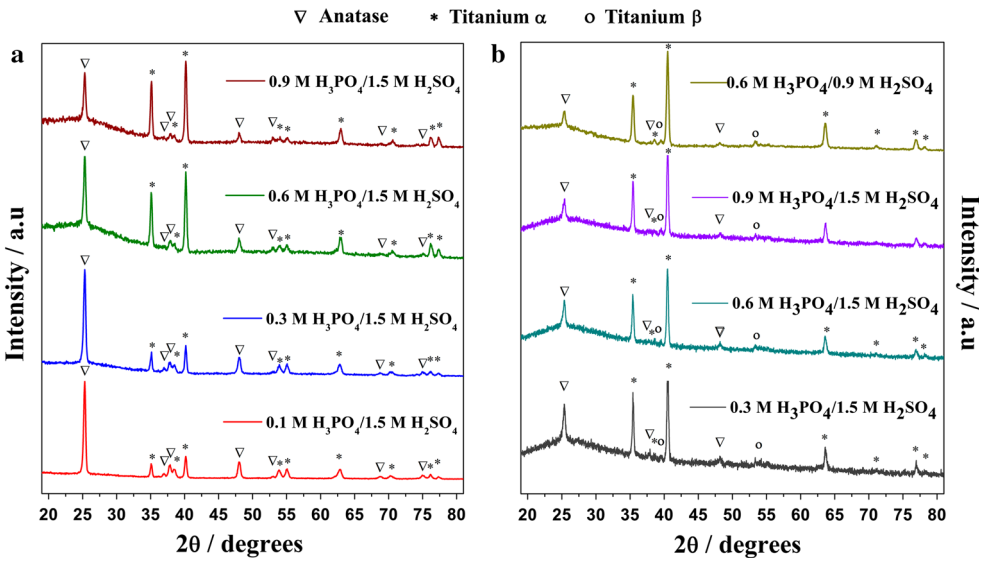

Fig. 3 XRD analysis of the anodic coatings obtained on **a** c.p Ti and **b** Ti6Al4V alloy at 35 mA cm^{-2}

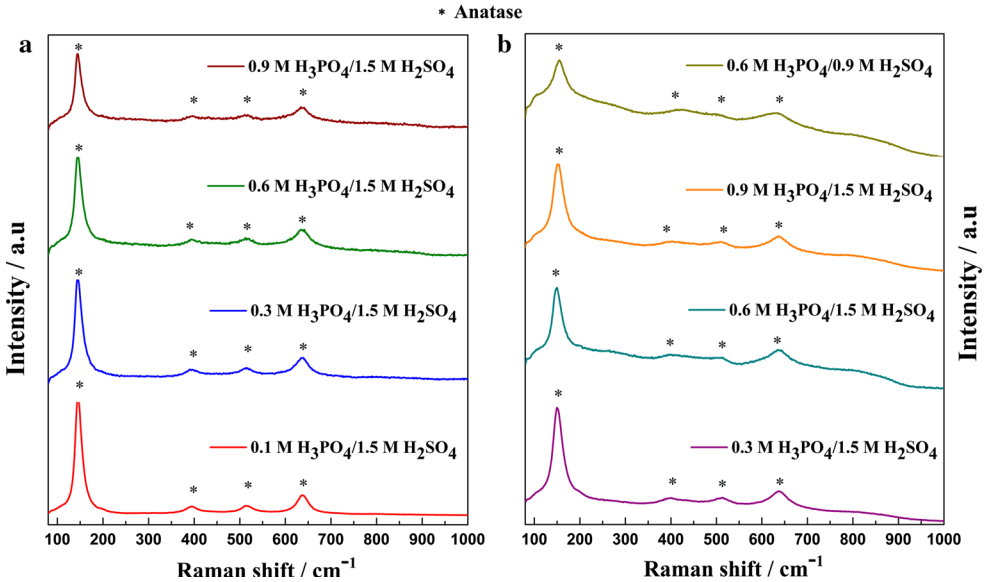

Fig. 4 Micro-Raman analysis of the anodic coatings obtained on **a** c.p Ti and **b** Ti6Al4V alloy at 35 mA cm^{-2}

H_2SO_4 whereas for Ti6Al4V alloy to samples treated with 0.3 M H_3PO_4/1.5 M H_2SO_4. Based on these results, the sample of c.p Ti treated with 0.1 M H_3PO_4/1.5 M H_2SO_4 was chosen to explore in more detail the interaction of the cells with the TiO_2 layer by using FIB transversal views. Pictures showed the way cells attach to the surface and how the basal body of the cell was in intimate contact with the material. A close interaction was also showed between filopodia not only in the surface but also deep in the pores of the anodized film (Fig. 7).

Osteoblasts labeled with actin allowed us to know in detail the interaction of the cells cytoskeleton and the treated surfaces (Fig. 8). This immunodetection assay allowed the identification of specific attachment points. Actin microfilaments in all directions conformed by extending lamellipodia and filopodia were observed in cells spreading over untreated c.p Ti and Ti6Al4V surfaces. On the other hand, cells over modified surfaces showed more filopodia and intimate attachment defined topographically by anchorage points organized according to the porous surfaces. Some spherical cells with a poor attach condition were also observed (Fig. 8). After observing these results, samples of c.p Ti treated with 0.1 M H_3PO_4/1.5 M H_2SO_4, and the Ti6Al4V treated with 0.3 M H_3PO_4/1.5 M H_2SO_4 and 0.6 M H_3PO_4/0.9 M H_2SO_4 were studied in more detail as these samples have the smaller pore sizes and they showed interesting results in terms of attachment and cytoskeleton organization.

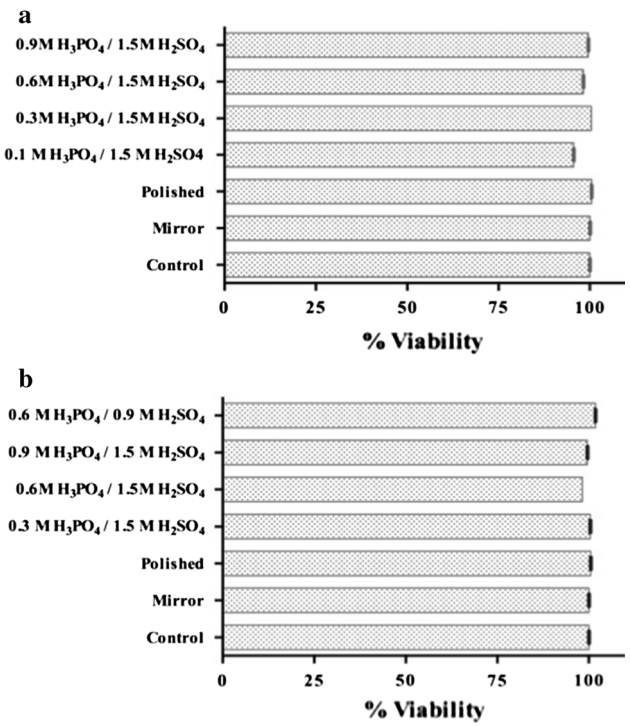

Fig. 5 Cellular viability of osteoblasts cells exposed to c.p Ti (**a**) and Ti6Al4V (**b**) specimens. *Bars* show the percentage of viability of cells after exposure to Ti specimens treated with different electrolytes in comparison with samples without treatment (polished and mirror) and cells seeded on plastic cell-culture (control). Experiments were done in triplicates, and the standard deviations are indicated

3.2.3 Cell proliferation

Alamar Blue assay was used to perform fluorescence emission measurement every 24 h for a total of 96 h. Results showed a curve of cell proliferation for osteoblasts that grew on the modified surfaces (Fig. 9). In all samples, cells showed a progressive growth with time; all samples retained the same growth pattern of control surfaces. The statistical analysis between all different groups of samples and their respective controls indicated no significant differences.

3.2.4 Cell mineralization

The ability of osteoblasts to mineralize the matrix produced during the differentiation process was determined by staining with Alizarine Red. This test was performed 4 and 7 days after cells were seeded on the samples. Osteoblasts that grew in the well of culture plate were assumed as positive control, and myoblasts growing in the same surface were the negative control. The addition of β sodium Glycerophosphate, acid ascorbic and dexamethasone allowed the differentiation process and subsequently mineralization. As expected, after 4 and 7 days it was possible to observe presence of nodules of mineralization in the positive control; however, in the negative control calcium deposits were not observed (Fig. 10).

After washing and fixing the cellular monolayer of osteoblasts that grew on c.p Ti and Ti6Al4V samples, they were examined microscopically to determine qualitative staining for calcium phosphate after 4 and 7 days of culture. In all of the samples, deposits of calcium phosphate were observed in a red dark color (Figs 11, 12).

4 Discussion

The surface features of a material that will be used as an implant, plays a critical role in the biological response from the host tissue. In this biointerface, proteins and cells interact to conduct tissue reparation [43]. Cellular behavior is greatly influenced by surface properties such as hydrophobicity, roughness, texture, and morphology. Specifically in the case of bone tissue, several studies using in vitro and in vivo assays, showed that rough surfaces produce better bone fixation than smooth surfaces, indicating that surface roughness has a direct effect on osteoblast attachment, proliferation and differentiation [44, 45].

There are different techniques that can be used to design surfaces in which parameters such as roughness and morphology are modified in order to improve tissue-material interaction. In this study, a protocol based on PEO method was standardized and consequently coating characteristics of surfaces such as oxide thickness, chemical composition, pore size, and roughness were produced in a reproducible way. Solutions composed of a mix of phosphoric and sulphuric acid were used and have been involved in the formation of porous structures in c.p Ti and Ti6Al4V alloy. Several studies have reported different combination of anodizing process parameters to obtain different topographies. Kim et al. [46] found that the composition of electrolyte determines not only the formation of microporous morphologies but also the incorporation of ions from electrolyte, which stimulate cell attachment and proliferation levels of cells. Macak et al. [47] obtained nanotubes multilayer in H_3PO_4/HF electrolytes and they concluded that the tube diameter can be varied changing the fluoride concentration and water content in the electrolyte. Similarly, in the present work it was found a specific combination of electrical conditions and electrolyte composition that can produce pores with controllable size and morphologies, which could help process of tissue reparation or regeneration.

It is widely reported that sparks phenomena are related to the nature and concentration of ions in the electrolyte, and that they cause the formation of larger pores [13]. During the anodizing process, the increase of cell voltage

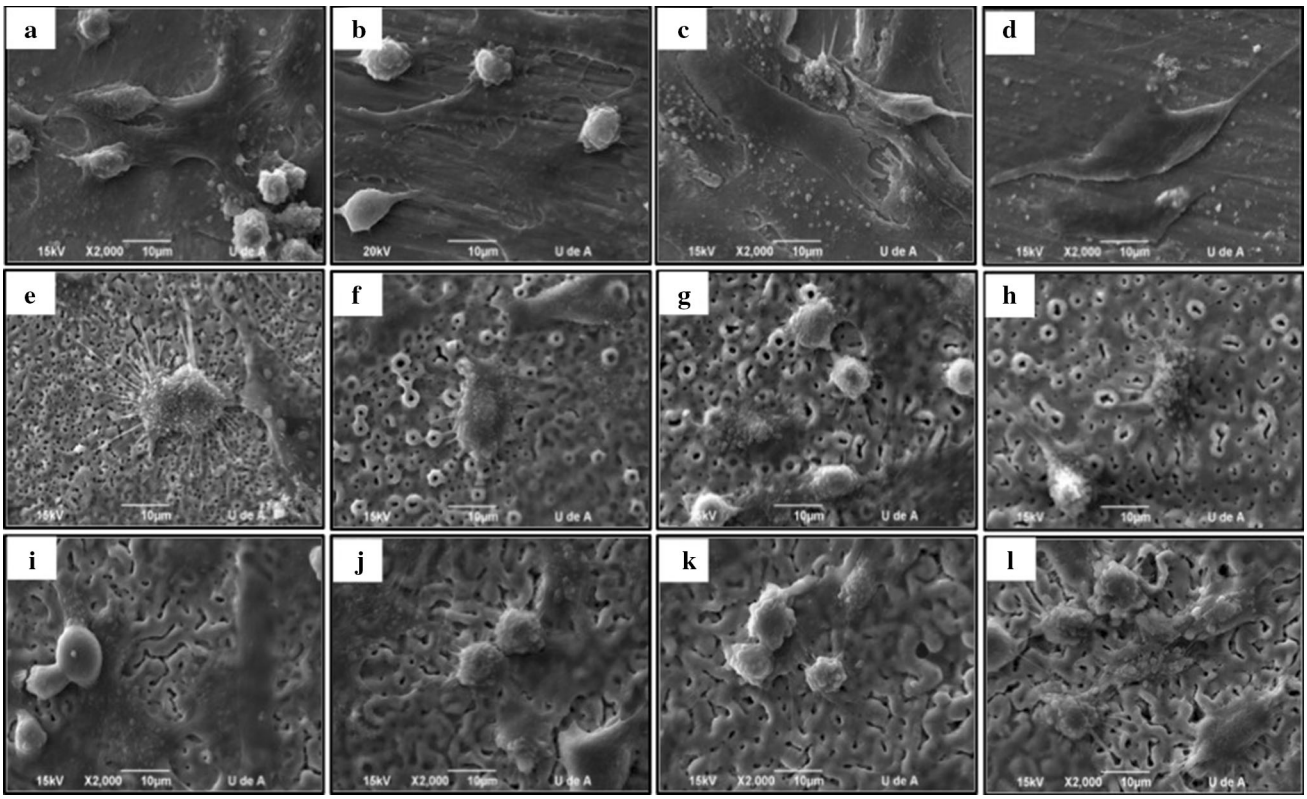

Fig. 6 SEM images of osteoblasts growing in different surfaces in which all of them were observed formation of monolayer **a** c.p Ti mirror grade, **b** c.p Ti polished 600, **c** Ti6Al4V mirror grade, **d** Ti6Al4V polished 600, **e** c.p Ti treated with 0.1 M H_3PO_4/1.5 M H_2SO_4, **f** c.p Ti treated with 0.3 M H_3PO_4/1.5 M H_2SO_4, **g** c.p Ti treated with 0.6 M H_3PO_4/1.5 M H_2SO_4, **h** c.p Ti treated with 0.9 M H_3PO_4/1.5 M H_2SO_4, **i** Ti6Al4V treated with 0.3 M H_3PO_4/1.5 M H_2SO_4, **j** Ti6Al4V treated with 0.6 M H_3PO_4/1.5 M H_2SO_4, **k** Ti6Al4V treated with 0.9 M H_3PO_4/1.5 M H_2SO_4, **l** Ti6Al4V treated with 0.6 M H_3PO_4/0.9 M H_2SO_4. Magnification ×2000

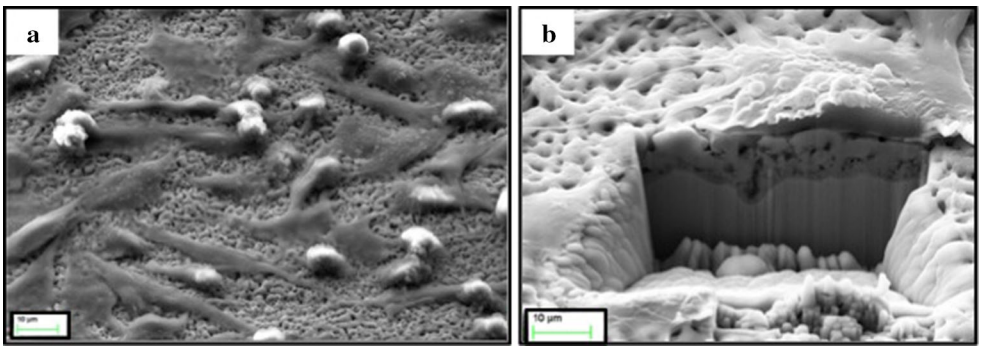

Fig. 7 Photographs showing the effect of cells growing in a modified surface of c.p Ti with 0.1 M H_3PO_4/1.5 M H_2SO_4: **a** selected zone with cells to make a cross section analysis; **b** Interaction between cell and surface pores was observed in the cross section; filopodio cross the porous layer promoting the adhesion to the surface

indicates thickening of the anodic layer, causing a high current density passing through the anodic layer [37]. Under these conditions, the current is located in the weakest areas of the anodic film to pass through it, producing breaks of larger sizes and more isolated on the layer, as it was reported by Petković et al. [48]. In addition, recent results described variations in the morphology of coatings formed galvanostatically on titanium by plasma electrolytic oxidation in phosphoric/sulphuric acid mixtures [49]. Initially, grooves and elongated pores are formed, as the PEO process continues and the sparks intensify, a morphological transition occurs, leading to the formation of circular pores. Formation of grooves took place from the onset of breakdown and continued at

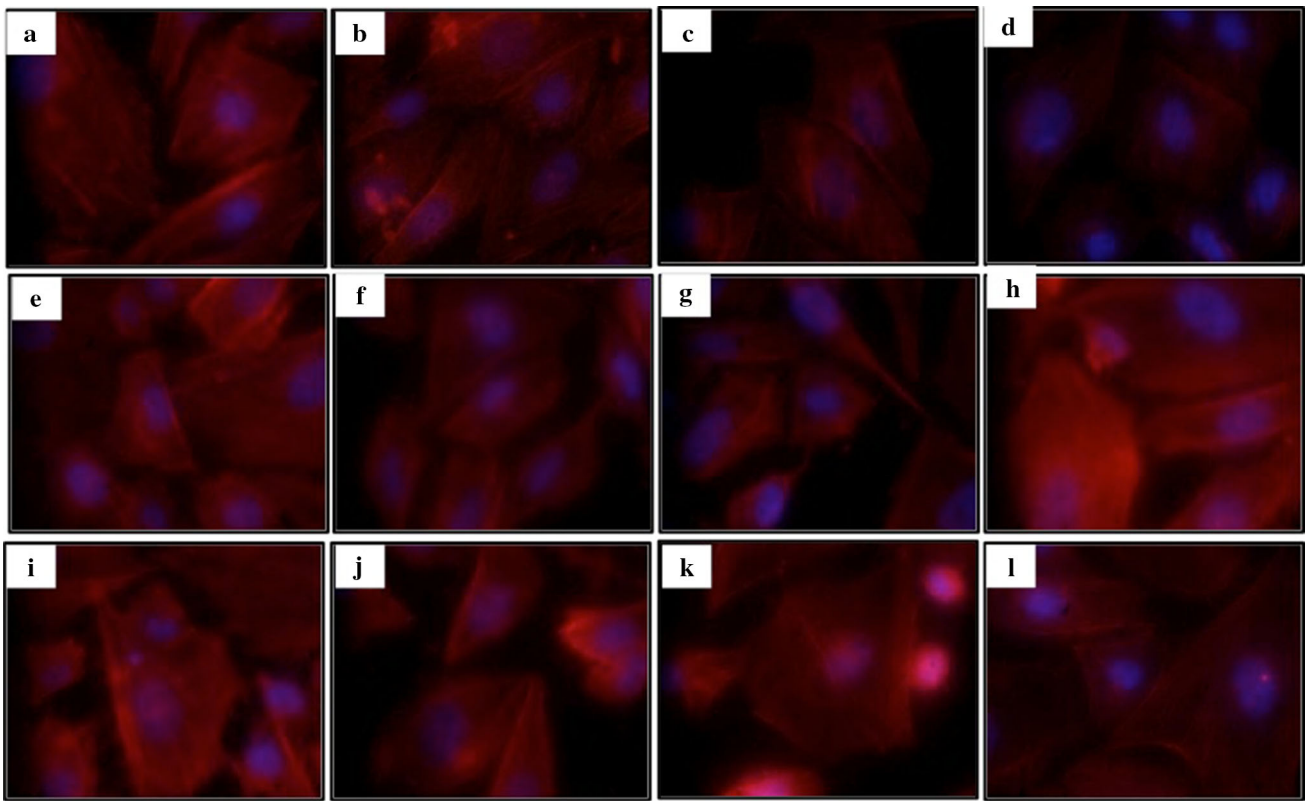

Fig. 8 Cytoskeleton of osteoblasts grew on modified surfaces were labeled with Phalloidin TRITC and DAPI for nucleus. Fluorescence microscopy images of cells showed an intimate contact between cells and the surfaces of the materials. **a** c.p Ti mirror grade, **b** c.p Ti polished 600, **c** Ti6Al4V mirror grade, **d** Ti6Al4V polished 600, **e** c.p Ti treated with 0.1 M H_3PO_4/1.5 M H_2SO_4, **f** c.p Ti treated with 0.3 M H_3PO_4/1.5 M H_2SO_4, **g** c.p Ti treated with 0.6 M H_3PO_4/1.5 M H_2SO_4, **h** c.p Ti treated with 0.9 M H_3PO_4/1.5 M H_2SO_4, **i** Ti6Al4V treated with 0.3 M H_3PO_4/1.5 M H_2SO_4) Ti6Al4V treated with 0.6 M H_3PO_4/1.5 M H_2SO_4, **k** Ti6Al4V treated with 0.9 M H_3PO_4/1.5 M H_2SO_4, **l** Ti6Al4V treated with 0.6 M H_3PO_4/0.9 M H_2SO_4. Magnifications ×40

voltages up to ~150 V in 0.1 M H_3PO_4/1.5 M H_2SO_4 and ~175 V in 0.9 M H_3PO_4/1.5 M H_2SO_4, with more prominent grooves formed in the latter electrolyte. The circular pores morphology appears to arise from fusion of the earlier formed grooves when a higher voltage is reached. Finally, it was found that the morphological transition is strongly related to the increased strength, density and shape of the sparks generated during the process [49]. These reports allows us to support the formation of elongated pores and grooves observed in this work around 160 and 180 V for all electrolytes, as showed in Fig. 6. The formation of grooved morphologies has been reported in other metals, including aluminum and magnesium [50, 51], although with no explanation for its occurrence other than a relation to the distribution of discharges over the coatings.

Roughness analysis reported in the Table 1 indicates the influence of the electrolyte concentration employed upon R_a values for all anodic coatings. These results are in agreement with others authors which have concluded that surface roughness, oxide crystallinity, and surface composition of anodic oxides were dependent on voltage, current density, and concentration of the electrolyte. Zhu et al. [13] investigated the effects of the electrolyte concentration and voltage on the characteristics of anodic oxides obtained on Ti and they found that the roughness varied as voltage, current density and concentration were increased. In addition, Li et al. [52] formed anodic oxide layers on Ti surfaces, by controlling the applied voltage and they concluded that as the applied voltage increased, the values of R_a slightly increased. As it was mentioned before, during the PEO process, the coating formed becomes thicker as a consequence of sparks and subsequent breakdown events that occur preferentially on unaffected regions of the coating, where the oxide is thinner. As a result of these series of events and reactions, the pore size and the roughness of the oxide layer could increase rapidly [48, 53], giving an explanation to morphological results showed in this work (Fig. 6).

It is known that the morphology of PEO coatings is directly related to breakdown features. During microdischarges, current is localized at weak points of the layer seeking a way

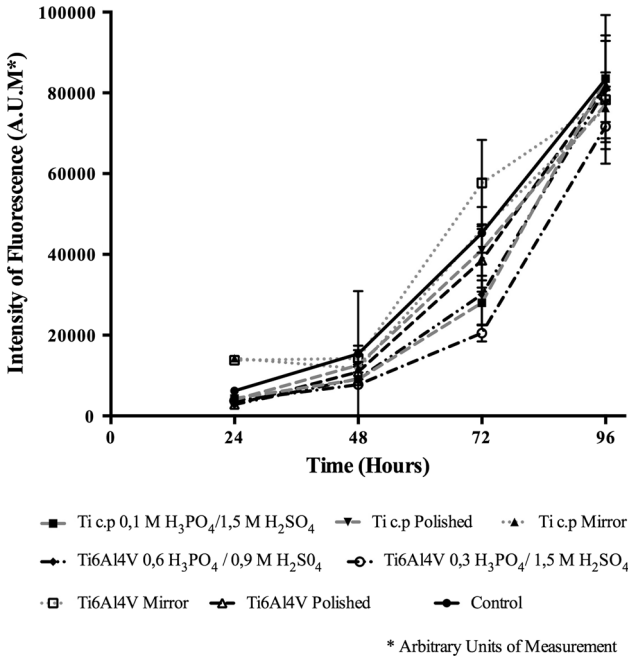

Fig. 9 Growth curves of osteoblasts obtained each 24 h during 4 days. Proliferation of osteoblasts in porous surfaces on c.p Ti and TiAl4V shows a similar tendency in comparison with the control and with samples non-treated. No significant differences were founded

through the coating, forming channels distributed all over the surface and consequently, roughness and pore size increase in these regions [23].

The EDS analysis indicated that the coatings obtained on c.p Ti are made of oxygen, phosphorus and titanium, while the coatings formed on Ti6Al4V alloy beside of these elements contain aluminium. Table 2 reports the component elements of the anodic coatings. The amount of phosphorous incorporated into the coatings during anodizing process depends strongly on the electrolyte composition, the higher the concentration of H_3PO_4, the higher the amount of P into the coatings, as expected [54]. However, sulphur was no detected by EDS; this could be due to relatively negligible amounts of sulphur species into the coatings. Lee et al. [26] formed anodic coatings on titanium in phosphoric/sulphuric acid mixtures, and found by X-ray photoelectron spectroscopy that phosphate species (H_2PO_4, PO_4^-, HPO_4^-, PO_3^-) were present in the coating.

XRD analysis (Fig. 3) showed peaks associated with substrate and anatase phase. It was seen that the intensities of anatase signals (at $2\theta = 26$) decrease when concentration of H_3PO_4 increased in the electrolyte employed during anodizing process. On the other side, we found that the average thickness values for each specimen (Table 2) were smaller as the concentration of H_3PO_4 increased in the electrolyte. The variations in thickness would explain the changes observed in anatase signals when the electrolyte concentration was modified. Although, this could be also altered because of the ionic species incorporated into the coatings from the electrolyte, which cause changes in the formation of the anatase and crystallization of the coatings [25, 26]. As was showed before in EDS analysis, the amount of P incorporated into the coatings increased as the concentration of H_3PO_4 increased in the electrolyte. These results are in agreement with others works; Naofumi et al. [55] found that the amount of S, B and P incorporated into coatings obtained on Ti depends on the concentration of the electrolyte used, and they also conclude that these species inhibited the crystallization of the coatings. On the other side, Cui et al. [56] reported the formation of amorphous anodic coatings on Ti in 2 M H_3PO_4 electrolyte at 100, 150 and 180 V and Diamanti et al. [57] affirmed that the crystallinity of coatings obtained in H_3PO_4 solution is lower due to the inhibitor effect of the phosphorous incorporated.

Micro-Raman spectra (Fig. 4) show the characteristic bands of anatase at 144, 397, 516 and 641 cm^{-1}, which are consistent with those reported in the literature for anodic coatings obtained on Ti alloys [40–42]. There is no evidence of other phases. The spectra also show that bands broaden as the concentration of H_3PO_4 in electrolytes

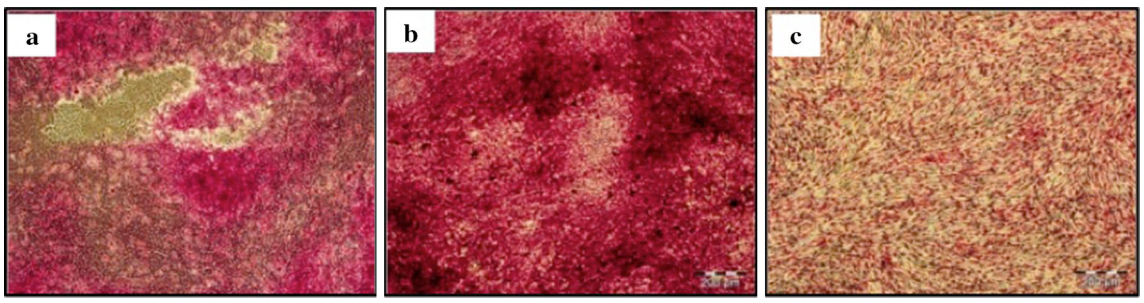

Fig. 10 Stain with Alizarin red for positive and negative controls in the mineralization assay. *Red stain* indicates mineralization zones. **a** Osteoblasts in presence of mineralization media after 4 days, **b** osteoblasts in presence of mineralization medium after 7 days. **c** Myoblasts growing in DMEM after 7 days (Color figure online)

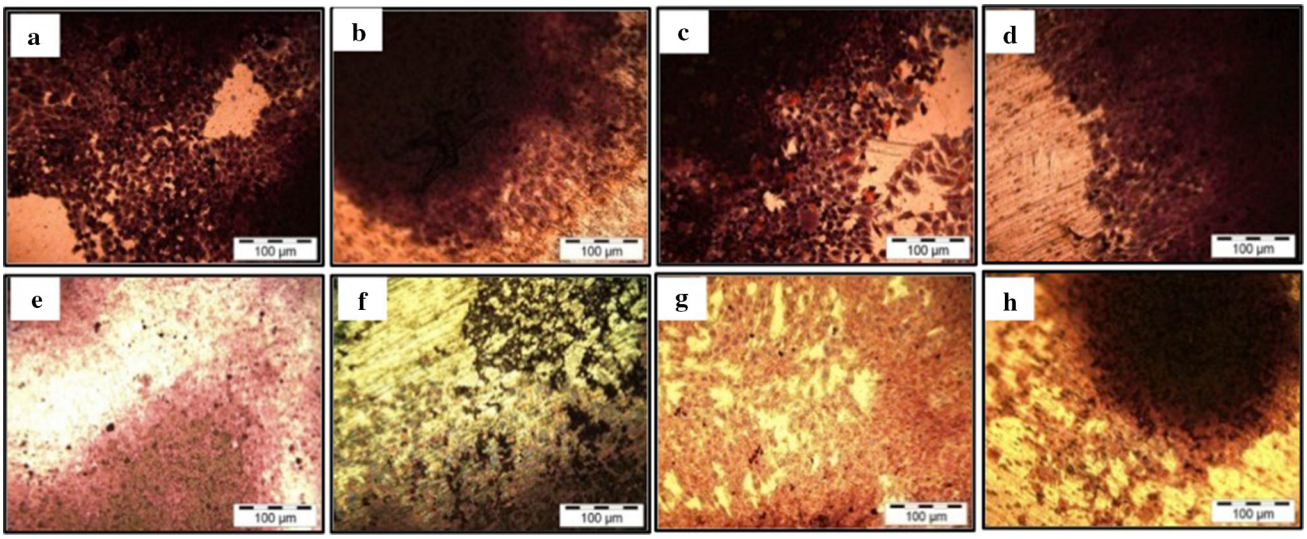

Fig. 11 Differentiation and mineralization activity of osteoblasts on surfaces without modified surface. Cells grew in presence of differentiation medium. *Red zones* were showed calcium deposition **a** c.p Ti mirror polished after 4 days, **b** c.p Ti polished 600 after 4 days, **c** Ti6Al4V mirror polished after 4 days, **d** Ti6Al4V polished 600 after 4 days, **e** c.p Ti mirror polished after 7 days, **f** c.p Ti polished 600 after 7 days, **g** Ti6Al4V mirror polished after 7 days, **h** Ti6Al4V polished 600 after 4 days. Magnification of ×10 (Color figure online)

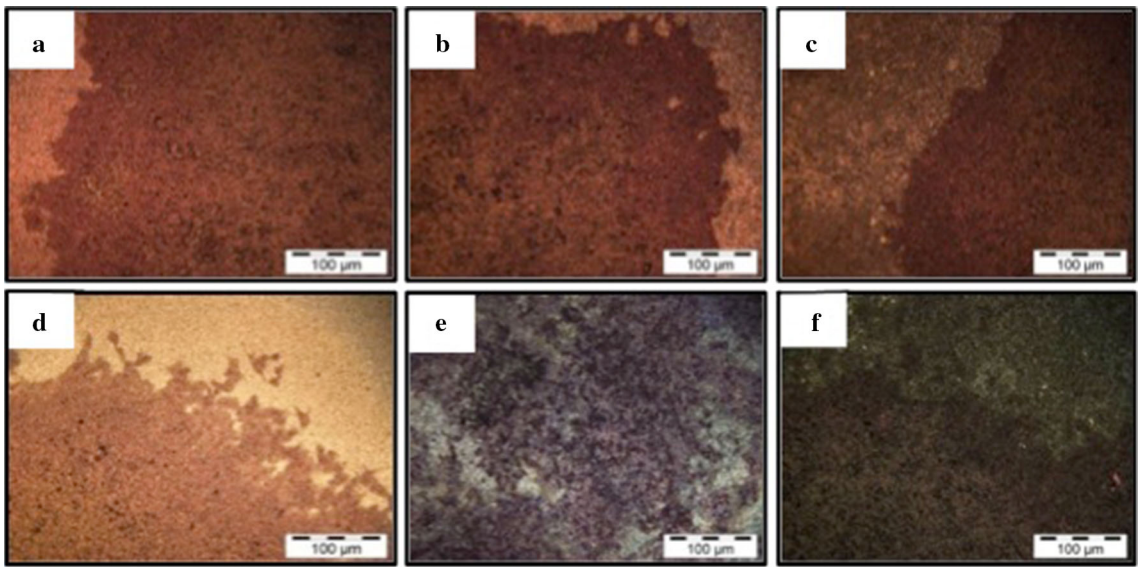

Fig. 12 Differentiation and mineralization activity of osteoblasts on modified surfaces of titanium detected through alizarin red stain in which zones of calcium deposition were identified as *red zones* in the surfaces. Cells grew in presence of differentiation medium. Measurements were taken after 7 and 14 days. **a** c.p Ti treated with 0.1 M H_3PO_4/1.5 M H_2SO_4 after 4 days, **b** c.p Ti treated with 0.3 M H_3PO_4/1.5 M H_2SO_4 after 4 days, **c** Ti6Al4V treated with 0.6 M H_3PO_4/0.9 M H_2SO_4 after 4 days, **d** c.p Ti treated with 0.1 M H_3PO_4/1.5 M H_2SO_4 after 7 days, **e** c.p Ti treated with 0.3 M H_3PO_4/1.5 M H_2SO_4 after 4 days, **f** Ti6Al4V treated with 0.6 M H_3PO_4/0.9 M H_2SO_4 after 7 days. Magnification of ×10 (Color figure online)

increases. These findings can be attributed to changes in the structure, in particular loss of crystallinity, similar to results obtained by XRD. Pankuch and co-workers [58], reported that the broadness of bands in the Raman spectra indicates a high disorder or amorphous nature of the coating.

In terms of biological response, cells grew appropriately in both materials, c.p Ti and Ti6Al4V with and without anodic modified surfaces, only a small variation was observed in the Ti6Al4V alloy sample polished to mirror finishing (Fig. 9); however, after statistical analysis, not significant difference was founded. This could be explained

because surfaces are not able to induce an increase of the population of the cell per se, but on the other hand this sort of surface modifications could promote the attachment and establishment of the osteoblast in the surface in an efficient way. These results showed also that modification of surfaces do not affect the biocompatibility of the material despite it was exposed to different aggressive and toxic solutions.

The results presented in the Fig. 6 showed a good response from the cells in the early process of adhesion onto the samples; that was confirmed by SEM analysis. These images provide information on the spatial distribution, cell morphology, cell–cell interaction and cell–material interaction. Cells that were grown on modified c.p Ti and Ti6Al4V showed a typical hexagonal shape, which is characteristic of osteoblasts in the same form that others studies have described [59]. After 48 h, osteoblasts adhered to all substrates by means of thin cytoplasmic digitations or filopodia but cells showed flattened and expanded cytoplasmic extensions over the entire material surface. Afterwards, cells formed multilayers in certain zones and appeared organized in nodules of various sizes and shapes. No particular orientation of cells was observed for modified samples; however, a special tendency was observed for polished samples in which cells grew in the same direction as the polishing lines. These results suggest that only the modification of the topography and morphology of the TiO_2 layer was not enough to induce a variation in cell proliferation. However, there are several studies in which it has been demonstrated that roughness, porosity and morphological characteristics have a direct influence on cell-to-cell interactions. Accordingly, a higher surface area/volume ratio, a larger area is available for cell attachment, this can also affect mass transport processes which play an important role for cell survival [43]. The results reported here support this statement due to differences in the configuration and cell organization of the cells that grew in modified surfaces in comparison with those growing on smooth surfaces. The first set of images showed more presence of filopodia that promotes a proper attachment of the cells onto TiO_2 surfaces. An increase in the number of cytoplasmic prolongations was also observed in the samples with smaller pore sizes indicating that roughness (R_a parameter) can affect cell attachment. Cell shape and phenotypic responses seem most pronounced when the scale of the surface feature is a fraction of the cell size (e.g., from tens to hundreds of nanometers) [60–63]. Similar results were observed in previous studies where not only the morphology but also the surface stiffness of the materials were considered as important factors in cellular behavior [64, 65]. Increased cell adhesion and spreading leads to cell proliferation and a moderate cell adhesion; the presence of rounded cell morphology could be associated with differentiated cellular function or non-affinity between cell and surfaces [66]. Lo et al. observed a rounded morphology in fibroblasts cultured on soft two-dimensional poly-acrylamide substrates (substrate stiffness 14 kPa) which was different when they compared the same cells growing on different substrates (substrate stiffness 30 kPa), which adopt a flat morphology [65]. In our case, some isolated cells with spherical morphology, different from the conventional cells were also present in all specimens. Although these cells did not exhibit good adherence to the surfaces these is not considered as a relevant because this cell population was also observed in the control specimens. Overall, there was a good interaction between cells and different morphologies on Ti specimens.

A tridimensional analysis of cells behavior on the modified surfaces was possible by using of FIB technique which allows to observe cell-material interactions in the anodized c.p Ti with an electrolyte of H_3PO_4 0.1 M/1.5 M H_2SO_4 in more detail. FIB images showed a network of partially interconnected pores in the TiO_2 layer that facilitates the cell–cell and cell–surface connections (Fig. 7). This result helps to understand that, unlike the low interaction that occurs with the smooth surfaces, anodic porous samples exhibit a more intimate interaction with cells because filopodias can be extended not only at superficial level but also inside of the layer. Additionally, porous anodic layers like those reported here produce more compliant Ti surfaces (lower surface stiffness) compared with a conventional bulk polished our machined rough surface. FIB images demonstrated that in the present work both micro and nano-porosity were produced, which indicates that there are two-scales of reduced surface stiffness. These lower stiffness surfaces can be assumed as a surface elasticity factor that is allowing easier interactions cells/material surfaces as some of the authors previously mentioned have found in their works.

Biointerface topography and, in particular topographic features can affect cell behavior and integrin-mediated cell adhesion, which is now evident from studies with fabricated topographical features [67–70]. The extent to which nano-topography influences cell behavior in vitro remains unclear, and investigations into this phenomenon are ongoing. The processes that mediate the cells reaction to nanoscale surface structures may be a direct result of the influence of surface topography or indirect in the case of a surface structure affected by composition, orientation, or conformation of the adsorbed extra cellular molecules (ECM components) [71–73]. Nano and microtopography is considered an important mediator of cellular adhesion and differential function, involving cellular behavior changes through the modulation of focal adhesion reinforcement and protein interaction kinetics. The process of adhesion and interaction between cells and surfaces is dependent on

some integrin-mediated cytoskeletal and some signal transduction molecules that can be visualized for different techniques through fluorescent stains. This is how by means of the stain of the actin of cells in the different samples it was possible to identify an organized structure of actin and the presence of specific attachment points (Fig. 8), which showed the connection between the cell and the material. This process is important because focal adhesion kinase (FAK), vinculin and actin are closely involved in the cytoplasmic domain of focal adhesion and in the process of transmission of signals. Stress fibers in cytoskeleton were also identified as well as products of the union of microfilaments which indicate a proper adherence of cells onto the substrate similar to what was reported by Okumura et al. [59]. In the same study they also investigated the initial attachment and subsequent behavior of human osteoblastic cells (Saos-2) to pure titanium (Ti), hydroxyapatite (HA), and glass; all these materials showed similar features to those obtained in this study where vinculin-positive focal adhesions continuously increased and were greater in comparison to those observed for HA in which a decrease of focal adhesion and stress fibers was observed [59].

The cytoskeleton configuration is a key factor as it can affect the deformability of the cells, whose stiffness could be influenced by the mechanical and chemical environments, including cell–cell and cell–ECM interactions [74, 75]. Cells are approximately between 10 and 50 μm in size, and they are comprised of many constituents. In the present work, actin staining showed a filament distribution of actin with microfilament inside the cytoplasm and especially at the border of the cells, irrespective of the surfaces, which is also consistent with the results of Wirth et al. [44]. Some spots at the cell borders indicated points of intimate contact between cells and material; this feature was also evident around the nucleus with a more diffuse intensity. Those spots are actually an indicative of bounds sites between actin filaments and membrane receptors. None qualitative difference between staining of surfaces was observed. Immunofluorescence images of adhesion proteins could not demonstrate differences between the modified surfaces, as it was also stated by Wirth et al. in their work about how the roughness and the chemistry of surfaces can affect the biological response of osteoblasts [44].

All these small-scale features of cells described above and their high sensitivity to mechanical stimulation help explaining cell sensitivity to nanostructured features of biointerfaces. A good example of the important role of mechanical loading in cell response is the well-known bone mechanobiology. In this process, osteoblasts and osteoclasts modulate their functions in terms of both the level and the direction of applied stress to bone [74, 75]. In the same sense, it can be stated in general that mechanical loading of cells induces deformation and remodeling, which influence many aspects of human health and disease. The modified layer obtained can improve the communication between cells due to the tridimensional features of these pores allowing the interchange of nutrients and signals between cells and environment. In addition, staining with alizarin red confirmed cell proliferation and differentiation typical from osteoblastic phenotype in all the samples of titanium; extracellular mineralized nodules were observed as it was reported in other studies [76].

In the dental field, implants with rough surfaces are more favorable in comparison with smooth ones because it can stimulate the process of integration with bone, however, the risk of having an oral diseases like periodontitis by bacterial growth could be high because of this surface. A possible solution to this problem could be the immobilization of antibiotics on the surfaces of the material.

5 Conclusions

The success of implants in orthopedic and dental applications will depend of the properties of implant materials and how those could affect cells attachment and differentiation, matrix production, and mineralization as well. Cells are able to sense substrate texture by changing their morphology, cytoskeleton configuration, and intra- and extracellular signaling. In the present study a controlled electrochemical process was developed to produce porous anodic coatings by modification of c.p Ti and Ti6Al4V alloy by use of PEO technique. Parameters such as time, voltage, current, nature and concentration of electrolytic solutions were established. In this way modified surfaces can be obtained in a predictable and reproducible manner. PEO technique combines chemical and morphological modification of titanium surfaces in a simple, controllable, and cost-effective method compared to other techniques such as plasma-spray.

The morphological and structural features of anodic coatings obtained were dependent on the composition of the electrolyte and electrical parameters used in the process. The coatings obtained on c.p Ti and Ti6Al4V in electrolytes with lower H_3PO_4 concentration showed morphology of circular pores, while the coatings obtained in electrolyte with higher concentration of acid presented elongated pores and grooves morphologies. XRD and Raman analysis indicated that anodic coatings are formed exclusively by anatase. In addition, the incorporation of species into the coatings, particularly phosphorous, depends on the concentration of H_3PO_4 in the electrolyte and affects the crystallinity of the coatings obtained on both alloys. This was manifested in changes of the intensities and broadness of bands in DRX and Raman.

All surfaces of c.p Ti and Ti6Al4V modified by using of PEO were biocompatible, indicating that anodizing did not affect the viability and survival of the cells. Biological assays indicates that cells grew on the modified samples of c.p Ti and Ti6Al4V, showed an intimate cell–cell and cell–material interaction; this aspect was better when these results were compared with unmodified c.p Ti and Ti6Al4V surfaces. Additionally, interfacial features between tissue and material such as topography and roughness play a crucial role in the osseointegration processes in terms of the attachment and quantity of tissue growing around the implant.

Finally, it can be stated that surface modifications of Ti implants in which a controlled topographical change is also involved, allow improvements of cells adhesion, increasing the contact area between cells and materials. However, it is not enough to accelerate the proliferation or migration of osteoblasts on those surfaces. The authors will continue working in a new approach to improve biological behavior by immobilization of proteins which can act as chemo-attractants to facilitate and stimulate the growth of bone cells around the implant.

Acknowledgments The authors are pleased to acknowledge the financial assistance of the "Departamento Administrativo de Ciencia, Tecnología e Innovación – COLCIENCIAS" through the Project 111545221209 and "Estrategia de Sostenibilidad 2013–2014 de la Universidad de Antioquia".

References

1. Oreffo RO, Triffitt JT. Future potentials for using osteogenic stem cells and biomaterials in orthopedics. Bone. 1999;25:5s.
2. Stevens MM. Biomaterials for bone tissue engineering. Biomater Bone Tissue Eng. 2008;11:18.
3. Oliva A, Della Ragione F, Salerno A, Riccio V, Tartaro G, Cozzolino A, D'Amato S, Pontoni G, Zappia V. Biocompatibility studies on glass ionomer cements by primary cultures of human osteoblasts. Biomaterials. 1996;17:1351.
4. Minagar S, Berndt CC, Wang J, Ivanova E, Wen C. A review of the application of anodization for the fabrication of nanotubes on metal implant surfaces. Acta Biomater. 2012;8:2875.
5. Zaffe D. Some considerations on biomaterials and bone. Micron. 2005;36:583.
6. Branemark PI, Hansson BO, Adell R, Breine U, Lindstrom J, Hallen O, Ohman A. Osseointegrated implants in the treatment of the edentulous jaw. Experience from a 10-year period. Scand J Plast Reconstr Surg. 1977;11(Suppl. 16):1.
7. Diamanti MV, Ormellese M, Pedeferri M. Alternating current anodizing of titanium in halogen acids combined with anodic spark deposition: morphological and structural variations. Corros Sci. 2010;52:1824.
8. Park Y-J, Shin K-H, Song H-J. Effects of anodizing conditions on bond strength of anodically oxidized film to titanium substrate. Appl Surf Sci. 2007;253:6013.
9. Chen C-C, Chen J-H, Chao C-G, Say WC. Electrochemical characteristics of surface of titanium formed by electrolytic polishing and anodizing. J Mater Sci. 2005;40:4053.
10. Kuromoto NK, Simão RA, Soares GA. Titanium oxide films produced on commercially pure titanium by anodic oxidation with different voltages. Mater Charact. 2007;58:114.
11. Chang CH, Lee HC, Chen CC, Wu YH, Hsu YM, Chang YP, Yang TI, Fang HW. A novel rotating electrochemically anodizing process to fabricate titanium oxide surface nanostructures enhancing the bioactivity of osteoblastic cells. J Biomed Mater Res A. 2012;100:1687.
12. Zhu X, Chen J, Scheideler L, Reichl R, Geis-Gerstorfer J. Effects of topography and composition of titanium surface oxides on osteoblast responses. Biomaterials. 2004;25:4087.
13. Zhu X, Ong JL, Kim S, Kim K. Surface characteristics and structure of anodic oxide films containing Ca and P on a titanium implant material. J Biomed Mater Res. 2002;60:333.
14. Zhu X, Kim K-H, Jeong Y. Anodic oxide films containing Ca and P of titanium biomaterial. Biomaterials. 2001;22:2199.
15. Ochsenbein A, Chai F, Winter S, Traisnel M, Breme J, Hildebrand HF. Osteoblast responses to different oxide coatings produced by the sol-gel process on titanium substrates. Acta Biomater. 2008;4:1506.
16. Cheng FT, Shi P, Man HC. Anatase coating on NiTi via a low-temperature sol–gel route for improving corrosion resistance. Scr Mater. 2004;51:1041.
17. Lee H, Song MY, Jurng J, Park Y-K. The synthesis and coating process of TiO_2 nanoparticles using CVD process. Powder Technol. 2011;214:64.
18. Yoshida R, Suzuki Y, Yoshikawa S. Syntheses of TiO_2(B) nanowires and TiO_2 anatase nanowires by hydrothermal and post-heat treatments. J Solid State Chem. 2005;178:2179.
19. Diamanti MV, Pedeferri MP. Effect of anodic oxidation parameters on the titanium oxides formation. Corros Sci. 2007;49:939.
20. Fadl-Allah SA, El-Sherief RM, Badawy WA. Electrochemical formation and characterization of porous titania (TiO2) films on Ti. J Appl Electrochem. 2008;38:1459.
21. Santos E, Kuromoto NK, Soares GA. Mechanical properties of titania films used as biomaterials. Mater Chem Phys. 2007;102:92.
22. Shokouhfar M, Dehghanian C, Montazeri M, Baradaran A. Preparation of ceramic coating on Ti substrate by plasma electrolytic oxidation in different electrolytes and evaluation of its corrosion resistance: part II. Appl Surf Sci. 2012;258:2416.
23. Stojadinović S, Vasilić R, Petković M, Zeković L. Plasma electrolytic oxidation of titanium in heteropolytungstate acids. Surf Coat Technol. 2011;206:575.
24. Li Y, Lee I-S, Cui F-Z, Choi S-H. The biocompatibility of nanostructured calcium phosphate coated on micro-arc oxidized titanium. Biomaterials. 2008;29:2025.
25. Oh H-J, Lee J-H, Jeong Y, Kim Y-J, Chi C-S. Microstructural characterization of biomedical titanium oxide film fabricated by electrochemical method. Surf Coat Technol. 2005;198:247.
26. Lee J-H, Kim S-E, Kim Y-J, Chi C-S, Oh H-J. Effects of microstructure of anodic titania on the formation of bioactive compounds. Mater Chem Phys. 2006;98:39.
27. Oh H-J, Lee J-H, Kim Y-J, Suh S-J, Lee J-H, Chi C-S. Surface characteristics of porous anodic TiO_2 layer for biomedical applications. Mater Chem Phys. 2008;109:10.
28. Yan Y, Sun J, Han Y, Li D, Cui K. Microstructure and bioactivity of Ca, P and Sr doped TiO_2 coating formed on porous titanium by micro-arc oxidation. Surf Coat Technol. 2010;205:1702.
29. Takebe J, Itoh S, Okada J, Ishibashi K. Anodic oxidation and hydrothermal treatment of titanium results in a surface that causes increased attachment and altered cytoskeletal morphology of rat bone marrow stromal cells in vitro. J Biomed Mater Res A. 2000;51:398.
30. Neupane MP, Park IS, Bae TS, Yi HK, Watari F, Lee MH. Biocompatibility of TiO_2 nanotubes fabricated on Ti using

different surfactant additives in electrolyte. Mater Chem Phys. 2012;134:536.
31. Sun J, Han Y, Cui K. Microstructure and apatite-forming ability of the MAO-treated porous titanium. Surf Coat Technol. 2008;202:4248.
32. ASTM Standard F67–13. Standar specification for unalloyed titanium, for surgical implant application. ASTM International: West Conshohocken; 2013.
33. ASTM Standard F136–12. Standard specification for wrought titanium-6aluminum-4vanadium eli (extra low interstitial) alloy for surgical implant applications. West Conshohocken: ASTM International; 2012.
34. ASTM Standard B600–11. Standard guide for descaling and cleaning titanium and titanium alloy surfaces. West Conshohocken: ASTM International; 2011.
35. Diamanti MV, Del Curto B, Pedeferri M. Interference colors of thin oxide layers on titanium. Color Res Appl. 2008;33:221.
36. Diamanti MV, Del Curto B, Masconale V, Passaro C, Pedeferri MP. Anodic coloring of titanium and its alloy for jewels production. Color Res Appl. 2012;37:384.
37. Yao Z, Jiang Y, Jia F, Jiang Z, Wang F. Growth characteristics of plasma electrolytic oxidation ceramic coatings on Ti–6Al–4V alloy. Appl Surf Sci. 2008;254:4084.
38. Wheeler JM, Collier CA, Paillard JM, Curran JA. Evaluation of micromechanical behaviour of plasma electrolytic oxidation (PEO) coatings on Ti–6Al–4V. Surf Coat Technol. 2010;204:3399.
39. ICDD, PDF-4, The International Centre for Diffraction Data, 2012.
40. Arsov LD, Kormann C, Plieth W. Electrochemical synthesis and in situ Raman spectroscopy of thin films of titanium dioxide. J Raman Spectrosc. 1991;22:573.
41. Prusi A, Arsov L, Haran B, Popov BN. Anodic behavior of Ti in KOH solutions ellipsometric and micro-raman spectroscopy studies. J Electrochem Soc. 2002;149:B491.
42. Arsov LD, Kormann C, Plieth W. In situ Raman spectra of anodically formed titanium dioxide layers in solutions of H_2SO_4, KOH, and HNO_3. J Electrochem Soc. 1991;138:2964.
43. Mikos AG, Sarakinos G, Lyman MD, Ingber DE, Vacanti JP, Langer R. Prevascularization of porous biodegradable polymers. Biotechnol Bioeng. 1993;42:716.
44. Wirth C, Grosgogeat B, Lagneau C, Jaffrezic-Renault N, Ponsonnet L. Biomaterial surface properties modulate in vitro rat calvaria osteoblasts response: roughness and or chemistry? Mater Sci Eng C. 2008;28:990.
45. Kung K-C, Lee T-M, Chen J-L, Lui T-S. Characteristics and biological responses of novel coatings containing strontium by micro-arc oxidation. Surf Coat Technol. 2010;205:1714.
46. Kim SE, Lim JH, Lee SC, Nam S-C, Kang H-G, Choi J. Anodically nanostructured titanium oxides for implant applications. Electrochim Acta. 2008;53:4846.
47. Macak JM, Hildebrand H, Marten-Jahns U, Schmuki P. Mechanistic aspects and growth of large diameter self-organized TiO_2 nanotubes. J Electroanal Chem. 2008;621:254.
48. Petković M, Stojadinović S, Vasilić R, Zeković L. Characterization of oxide coatings formed on tantalum by plasma electrolytic oxidation in 12-tungstosilicic acid. Appl Surf Sci. 2011;257:10590.
49. Galvis OA, Quintero D, Castaño JG, Liu H, Thompson GE, Skeldon P, Echeverría F. Formation of grooved and porous coatings on titanium by plasma electrolytic oxidation in H_2SO_4/H_3PO_4 electrolytes and effects of coating morphology on adhesive bonding. Surf Coat Technol. 2014.
50. Shen D, Li G, Guo C, Zou J, Cai J, He D, Ma H, Liu F. Microstructure and corrosion behavior of micro-arc oxidation coating on 6061 aluminum alloy pre-treated by high-temperature oxidation. Appl Surf Sci. 2013;287:451.
51. Zhao L, Cui C, Wang Q, Bu S. Growth characteristics and corrosion resistance of micro-arc oxidation coating on pure magnesium for biomedical applications. Corros Sci. 2010;52:2228.
52. Li L-H, Kong Y-M, Kim H-W, Kim Y-W, Kim H-E, Heo S-J, Koak J-Y. Improved biological performance of Ti implants due to surface modification by micro-arc oxidation. Biomaterials. 2004;25:2867.
53. Cheng Y, Wu F, Matykina E, Skeldon P, Thompson GE. The influences of microdischarge types and silicate on the morphologies and phase compositions of plasma electrolytic oxidation coatings on Zircaloy-2. Corros Sci. 2012;59:307.
54. Ferdjani S, David D, Beranger G. Anodic oxidation of titanium in phosphoric acid baths: phosphorus incorporation into the oxide. J Alloy Compd. 1993;200:191.
55. Ohtsu N, Komiya S, Kodama K. Effect of electrolytes on anodic oxidation of titanium for fabricating titanium dioxide photocatalyst. Thin Solid Films. 2013;534:70.
56. Cui X, Kim HM, Kawashita M, Wang L, Xiong T, Kokubo T, Nakamura T. Preparation of bioactive titania films on titanium metal via anodic oxidation. Dent Mater. 2009;25:80.
57. Diamanti MV, Spreafico FC, Pedeferri MP. Production of anodic TiO_2 nanofilms and their characterization. Phys Procedia. 2013;40:30.
58. Pankuch M, Bell R, Melendres CA. Composition and structure of the anodic films on titanium in aqueous solutions. Electrochim Acta. 1993;38:2777.
59. Okumura A, Goto M, Goto T, Yoshinari M, Masuko S, Katsuki T, Tanaka T. Substrate affects the initial attachment and subsequent behavior of human osteoblastic cells (Saos-2). Biomaterials. 2001;22:2263.
60. Vogler EA, Akhlesh L, Raúl José M-P. Surface modification for biocompatibility. Engineered biomimicry. Boston: Elsevier; 2013. p. 189–220.
61. Flemming RG, Murphy CJ, Abrams GA, Goodman SL, Nealey PF. Effects of synthetic micro- and nano-structured surfaces on cell behavior. Biomaterials. 1999;20:573.
62. Aparicio C, Javier Gil F, Fonseca C, Barbosa M, Planell JA. Corrosion behaviour of commercially pure titanium shot blasted with different materials and sizes of shot particles for dental implant applications. Biomaterials. 2003;24:263.
63. Martínez E, Engel E, Planell JA, Samitier J. Effects of artificial micro- and nano-structured surfaces on cell behaviour. Ann Anat. 2009;191:126.
64. Discher DE, Janmey P, Wang Y-L. Tissue cells feel and respond to the stiffness of their substrate. Science. 2005;310:1139.
65. Lo C-M, Wang H-B, Dembo M, Wang Y-L. Cell movement is guided by the rigidity of the substrate. Biophys J. 2000;79:144.
66. Mooney D, Hansen L, Vacanti J, Langer R, Farmer S, Ingber D. Switching from differentiation to growth in hepatocytes: control by extracellular matrix. J Cell Physiol. 1992;151:497.
67. Ward MD, Hammer DA. A theoretical analysis for the effect of focal contact formation on cell-substrate attachment strength. Biophys J. 1993;64:936–59.
68. Balaban NQ, Schwarz US, Riveline D, Goichberg P, Tzur G, Sabanay I, Mahalu D, Safran S, Bershadsky A, Addadi L. Force and focal adhesion assembly: a close relationship studied using elastic micropatterned substrates. Nature Cell Biol. 2001;3:466.
69. Takagi J, Petre BM, Walz T, Springer TA. Global conformational rearrangements in integrin extracellular domains in outside-in and inside-out signaling. Cell. 2002;110:599.
70. Biggs MJP, Richards RG, Dalby MJ. Nanotopographical modification: a regulator of cellular function through focal adhesions. Nanomedicine. 2010;6:619.
71. Dalby MJ, Gadegaard N, Tare R, Andar A, Riehle MO, Herzyk P, Wilkinson CD, Oreffo RO. The control of human mesenchymal cell differentiation using nanoscale symmetry and disorder. Nat Mater. 2007;6:997.

72. Andersson AS, Brink J, Lidberg U, Sutherland DS. Influence of systematically varied nanoscale topography on the morphology of epithelial cells. IEEE Trans NanoBiosci. 2003;2:49.
73. Martines E, Seunarine K, Morgan H, Gadegaard N, Wilkinson CDW, Riehle MO. Superhydrophobicity and superhydrophilicity of regular nanopatterns. Nano Lett. 2005;5:2097.
74. Hench LL, Thompson I. Twenty-first century challenges for biomaterials. J R Soc Interface. 2010;7:S379.
75. Bao G, Suresh S. Cell and molecular mechanics of biological materials. Nat Mater. 2003;2:715.
76. Yang Y, Kim K-H, Ong JL. A review on calcium phosphate coatings produced using a sputtering process—an alternative to plasma spraying. Biomaterials. 2005;26:327.